50th AIAA Aerospace Sciences Meeting including the New Horizons Forum and Aerospace Exposition
09 - 12 January 2012, Nashville, Tennessee

AIAA 2012-1079

Vortex Formation of Freely Falling Plates

Hui Wan* and Haibo Dong† and Zongxian Liang‡
Department of Mechanical and Materials Engineering, Wright State University, Dayton, OH, 45435, USA

The problem of a freely fluttering or tumbling plate is studied using direct numerical simulation (DNS) by solving the Navier-Stokes equations and body dynamic equations simultaneously. The vortex formation in the transient process and periodic motion of the falling plate is investigated. The correlation between the body kinematics and force generation is discussed. The different roles played by viscous force in fluttering and tumbling plates are also pointed out.

Nomenclature

$\mathbf{\Omega}$	Angular velocity of the body, rad/s
$\mathbf{F}$	Force on the body, per unit width, N/m
$\mathbf{u}$	Velocity vector, non-dimensional
$\mathbf{V_c}$	Center velocity of the body, non-dimensional
F_r	Froude number
g	Gravitational acceleration, m/s^2
h	Thickness of body, m
I	Moment of Inertia, per unit width
L	Characteristic length, m
M	Mass per unit width, kg/m
p	Pressure, non-dimensional
R_e	Reynolds number
t	Time, non-dimensional
U_0	Characteristic velocity, m/s

Symbols

ρ_f	Density of fluid, kg/m^3
ρ_s	Density of body, kg/m^3
$\boldsymbol{\tau}$	Torque on the body, per unit width

I. Introduction

FREE falling of a plate in fluid is a classical problem,[1] which still attracts a lot of studies.[2,3] As long as the Reynolds number is high enough,[4] a plate will flutter or tumble depending on the moment of inertia (or equivalently, Froude number). Belmonte et al.[5] conducted experimental studies on thin flat strips falling in a vertical cell. They categorized the Froude number at which the transition from flutter to tumble occurs. Anderson et al.[6,7] analyzed the transitions between fluttering and tumbling using vorticity-stream function formulation and ODE dynamic equations based on fluid force model. Mittal et al.[8] numerically studied pinned freely rotating plates, which have only one degree of freedom. Relatively few direct numerical simulations on a freely falling plate can be found.[9,10] Specifically, the transient process of the freely falling is merely discussed in literatures.[11] The current paper will conduct direct numerical simulation on a freely falling plate and its induced flow field, for both transient process and periodic motion. The correlation between the plate motion, generated vortices, and aerodynamic forces will be studied.

*Research Associate, AIAA Member, hui.wan@wright.edu.
†Associate Professor, AIAA Associate Fellow, Corresponding author, haibo.dong@wright.edu
‡Graduate Student, liang.5@wright.edu

II. Method

II.A. Math and Equations

In the problem of a freely falling plate, the flow field is solved by non-dimensional incompressible Navier-Stokes equations as follows:

$$\nabla \cdot \mathbf{u} = 0 \tag{1}$$

$$\frac{\partial \mathbf{u}}{\partial t} + \mathbf{u} \cdot \nabla \mathbf{u} = -\nabla p + \frac{1}{R_e} \nabla^2 \mathbf{u} \tag{2}$$

where $\mathbf{u}$ is the velocity vector, p is the pressure, t is the non-dimensional time, and R_e is the Reynolds number. The Navier-Stokes equations are discretized using a cell-centered, collocated arrangement of the primitive variables ($\mathbf{u}$, p). A second-order, Adams-Bashforth scheme is employed for the convective term, and the diffusion term is discretized using an implicit Crank-Nicholson scheme. More details about the immersed boundary method can be found in previous publications.[12,13] The dynamic equations of a two-dimensional rigid body are:

$$M \frac{d\mathbf{V}_c}{dt} = \mathbf{F}(t) \tag{3}$$

$$I \frac{d\mathbf{\Omega}}{dt} = \boldsymbol{\tau}(t) \tag{4}$$

where $\mathbf{V}_c$(U,V) and $\mathbf{\Omega}$ are the translational velocity at mass center, and angular velocity of the body respectively. M is the mass of the body per unit width in spanwise direction, and I is the moment of inertia. $\mathbf{F}$ is the total force applied on the body including the aerodynamic force, and buoyancy-corrected gravitational force. The $\boldsymbol{\tau}$ is the moment with respect to the mass center. Here it has been assumed that aerodynamic moment is the only source of $\boldsymbol{\tau}$. Three non-dimensional parameters can be obtained from the variables governing the freely falling plate problem.[2] They are the thickness-over-length ratio h/L, the Reynolds number $R_e = \rho_f U_0 / \nu$, and the modified Froude number $F_r = (\frac{M}{\rho_f L^2})^{\frac{1}{2}}$ for a two-dimensional body. The ν in the definition of Reynolds number is kinematic viscosity of fluid. The characteristic speed U_0 used to define Reynolds number can be roughly estimated from the balance between the aerodynamic drag and buoyancy-corrected gravity,[6,11] which leads to $U_0 = \sqrt{2(\rho_s/\rho_f - 1)hg}$, where ρ_f and ρ_s are the fluid and solid density respectively, and g is the gravitational acceleration. The characteristic speeds of falling plates varies with density. The Navier-Stokes equations and body dynamic equations are implicitly coupled and solved iteratively. The computational domain extends to an overall region of 30 by 30 chord-lengths in x and y directions respectively. A dense region of 15 by 12 is placed in the center of the computational domain. The grid spacing in the dense region is $\Delta x = \Delta y = 0.013$.

III. Results

Preliminary study is conducted to compare our simulation with experimental results of Belmonte et al.,[5] using a flat plate with rounded edges. The thickness-over-length ratio h/L is 0.06, and the Froude number F_r is 0.45. The trajectory of the plate is shown in figure 1(b), which is very similar to that in figure 1(a) of Ref.5. The vortex structure from DNS is shown in figure 1(d), carrying good similarity compared with the experimental result shown in figure 1(c) in Belmonte et al.[5] In the following discussion, an elliptical plate is used in DNS, as sketched in figure 2. The inclination angle is defined as the angle between the horizontal direction and the major axis of the plate. In the current study, the thickness-to-length ratio h/L of the elliptical plate is 1/8. The Froude number and Reynolds number for the fluttering plate are 0.45 and 140 respectively. For the tumbling plate, we have used $F_r = 0.89$ and $R_e = 420$. In all cases, the plates are released with zero initial impulse (i.e. zero translational and rotational velocities).

III.A. Fluttering and tumbling plates

A plate released from rest at non-zero initial inclination angle and with sufficient high Reynolds number will end up with fluttering (low F_r), tumbling (high F_r) or chaotic motion (intermediate F_r) once the transition fades out. The trajectories of fluttering and tumbling plates are shown in figure 3. The initial inclination angle (θ_0) of the fluttering plate in figure 3(a) is set to 45° or 75°. After the plate is released from rest, it immediately slides obliquely along a short straight path, instead of falling vertically. As pointed out by

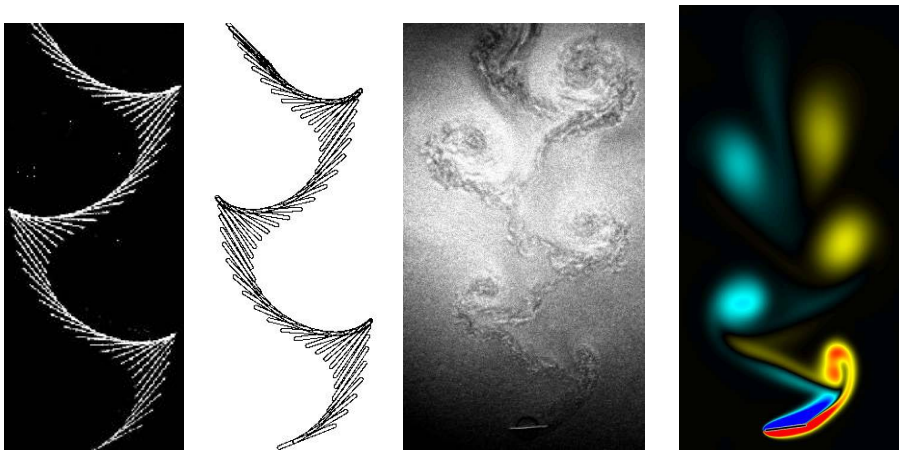

(a) Trajectory in Belmonte et al. (b) Trajectory in current study (c) Aluminum particle visualization in Belmonte et al. (d) Vortex structure from DNS

Figure 1. Fluttering of a flat plate, comparison between DNS simulation and experimental results from Belmonte et al.(1998).

Jones et al.,[11] this phenomenon is important since it shows that the aerodynamic response to the motion of the plate driven by the gravity is instantaneous and builds up immediately. In figure 3(a), the plate with 45° initial inclination angle experiences a shorter transient process before steady fluttering is obtained, compared to the plate released from 75°. Once the steady fluttering is approached, the trajectories of the two plates show similar fluctuation in horizontal direction and similar descending in vertical direction. The plate with 75° initial angle descends a longer distance only because it drops faster (as shown the vertical speed V in figure 4(a)) in the transient stage. Figure 3(b) presents two tumbling plates with initial inclination angle of 45° and −75° respectively. The plate with −75° initial angle starts to tumble immediately after it is released. The plate with 45° initial angle experiences a longer transient process. It starts with fluttering first, followed by an acceleration in vertical direction, and eventually settles down into tumbling. The descending pathes of both cases are almost in parallel, with an angle around 25.5° relative to the X-axis.

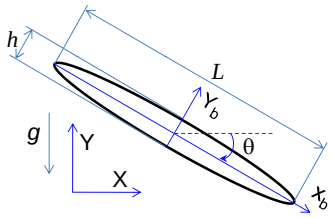

Figure 2. Coordinate system

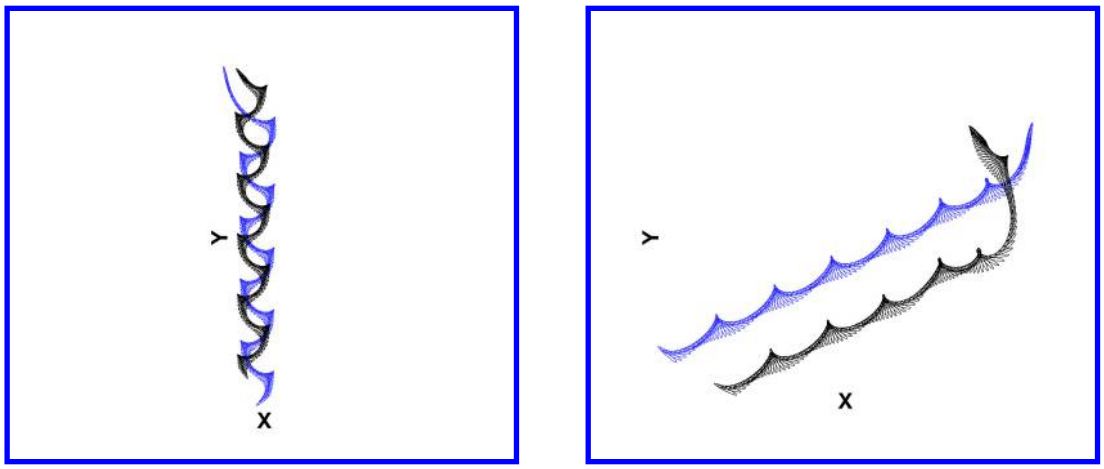

(a) Fluttering plate, $F_r = 0.45$, initial angle 45° (black) and 75° (blue)

(b) Tumbling plate, $F_r = 0.89$, initial angle 45° (black) and −75° (blue)

Figure 3. Trajectories of fluttering and tumbling plates

The phase plots of fluttering and tumbling plates are shown in figure 4.

For both fluttering and tumbling cases, once the initial transient process fades out, the terminal states of the plates with the two initial angles selected in this paper will approach to the same limit cycle. In figure 4(a), the plate released from 45° initial inclination angle shows a smaller initial cycle during transient stage, then approaches to the limit cycle with increased magnitude of velocity. Hence, from the transient process to periodic fluttering, the plate extracts energy from the surrounding fluid. On the contrary, the plate with 75° initial inclination angle gains high velocity swiftly after release, as shown by the initial cycle with larger size. The extra energy obtained during the transient process is dissipated to the surrounding fluid by aerodynamic damping. A similar damping phenomenon can also be seen in the tumbling plate as shown in figure 4(b).

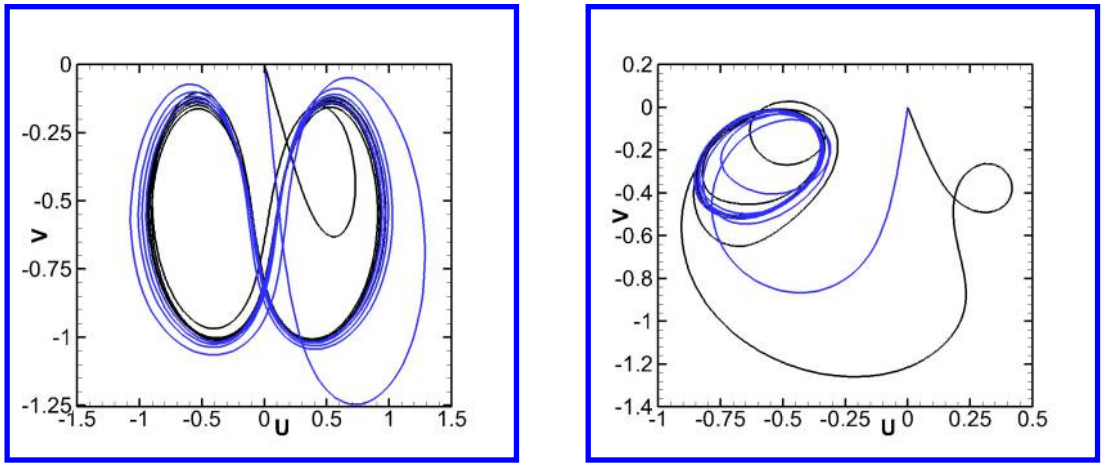

(a) Flutter: initial angle 45° (black) and 75° (blue)

(b) Tumble: initial angle 45° (black) and −75° (blue)

Figure 4. Phase plots of fluttering and tumbling plates

III.B. Transient process prior to fluttering

Figure 5 shows the velocity of the plates in transient process with initial angle 45° (solid line) and 75° (dashline) respectively. During the initiation of the plate falling, it is appropriate to assume that the flow is irrotational, thus the force on the plate is dominated by the reaction from the displaced fluid (added mass). Note the added mass is related to the plate density and initial inclination angle in the global X-Y coordinate system. Thus, the sideways and downward forces resulting from the added mass effect and the resulting direction of sliding (the slope of trajectory) right after release depend on the initial angle θ_0 and the Froude number. In Ref.11, the sideways and downward forces on a zero-thickness flat plate have been formulated, which may not be applied to plates with finite thickness and arbitrary cross-section. However, for a thin elliptical plate in the current study, the general trend of force variation with initial angle may still hold. Thus, we have $\mathrm{F_X} \sim f_X(1/F_r)\sin 2\theta_0$ and $\mathrm{F_Y} \sim -Mg + f_Y(1/F_r)\cos^2\theta_0$, where f_X and f_Y stand for certain functions of Froude number and body geometry in X and Y direction respectively. For a plate with known F_r, the maximum sideways force is obtained when the initial inclination angle is ±45°, and is zero when θ_0 is 0° or ±90°. The minimum downwards force (maximum drag from fluids) is at initial angle 0°, and increases in magnitude as the initial angle increases from horizontal to vertical, where the fluid plays minimum role. For the plate with −75° initial angle, $\mathrm{F_Y}$ is far greater than $\mathrm{F_X}$, giving rise to the fast acceleration in Y-direction of the plate. Also note right after release, both the horizontal and vertical speeds increase linearly with respect to time. The vorticity contours in the transient process of a plate released at 45° is shown in figure 6. Figure 6(a) shows nearly symmetric vortex layer on the lower and upper sides of the plate immediately after release, since the plate moves along the direction of its initial

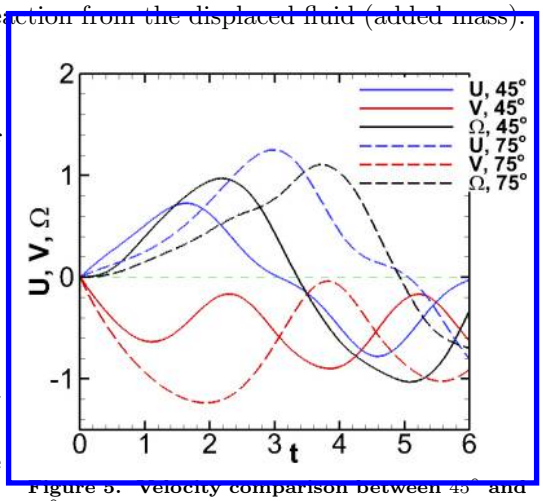

Figure 5. Velocity comparison between 45° and 75° release.

inclination at this moment. Since |V| > |U|, a stagnation point will be generated under the leading edge of the plate. The symmetry of the vortex layer is broken in figure 6(b), in which the angular velocity of the plate starts to increase. In figures 6(c) and 6(d), the plate reaches its maximum vertical and horizontal speed respectively after release. Note the attached vorticity layers fully cover the upper and lower side of the plate, indicating translation dominated motion by far. Also, a trailing edge vortex sheet (starting vortex) emanated from the lower surface of the plate. The vorticity in figure 6(e) is taken when the angular velocity of the plate is the maximum in magnitude, at which most of the upper surface of the body is covered by a leading edge vortex (LEV), while the wake is formed by the stretched trailing edge vortex (TEV). Above the trailing edge, there is a channel sandwiched between the wake and the short tail of the LEV, in which the vorticity is around zero but the velocity is locally high. This high speed channel and its direction relative to the body orientation actually play an important role in the motion, as will be seen later. Figure 6(f) is taken when the angular velocity of the plate is around zero. The high speed channel is close to the mid-chord of the plate, indicating the small torque experienced by the plate at this instant.

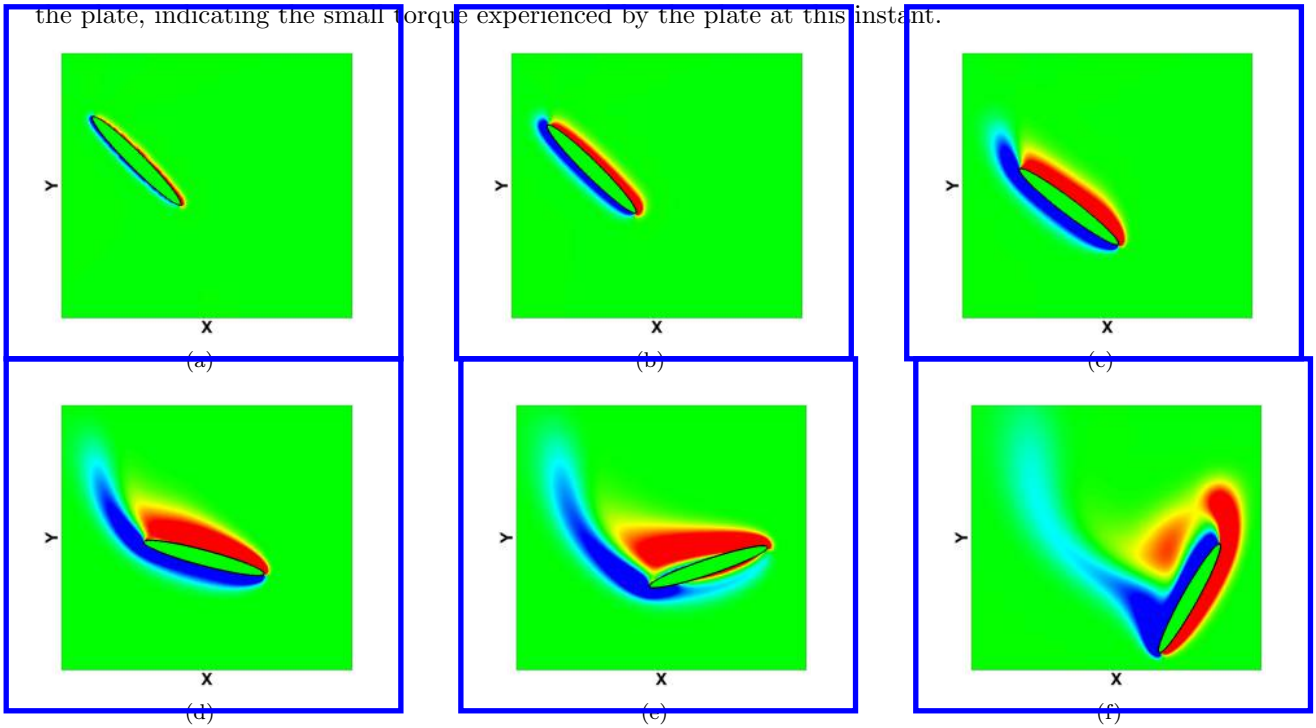

Figure 6. Vortices structure generated in transient process prior to fluttering, $F_r = 0.45$, $\theta_0 = 45°$.

III.C. Steady fluttering

The time course of velocity components of the plate in steady fluttering is shown in figure 7(a). The horizontal velocity U and the angular velocity Ω oscillate around a mean value of zero, while the vertical velocity V shows a nearly sinusoidal history with a non-zero mean value, indicating a periodic and steady falling of the plate. The correlation between the horizontal velocity U and angular velocity Ω is obvious. The plate swings symmetrically with respect to its longitudinal direction of motion, reaching its maximum location in lateral direction and maximum inclination angle almost simultaneously. In addition, the peaks of angular velocity correlate with the minima (in magnitude) of vertical speed. Hence Ω is maximum when the descending speed is minimum.

Figure 8 presents the vortices development of a fluttering plate when the steady fluttering is obtained. The corresponding plate locations of the labeled points are shown in figure 7(b), which presents the trajectory of plates in steady fluttering. Figure 8(a) shows the vorticity when the plate is with zero angular velocity, at which an LEV (red) starts to develop. The growth and behavior of this LEV influence the flow structure as well as the aerodynamic loading during dynamic stall. It can be seen that the clockwise vortex generated in the previous cycle has been shed, by which a new shear layer with counterclockwise vorticity is induced on the upper surface of the plate. Figure 8(b) corresponds to the minimum effective angle of attack (the relative angle between the plate velocity and plate inclination), which is around 15°. The LEV and previously

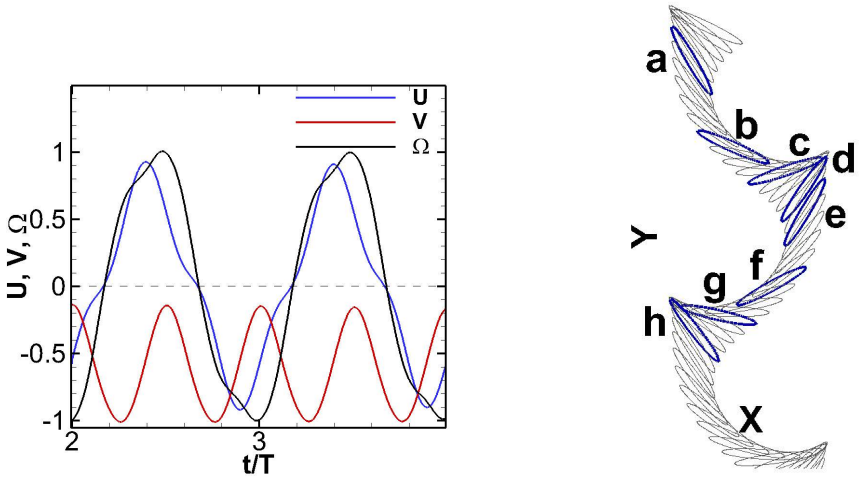

(a) Time history of velocity components (b) Plate trajectory

Figure 7. A plate in steady fluttering, $F_r = 0.45$, $\theta_0 = 45^\circ$

induced shear layer are merged to form a strong shear layer covering the whole upper surface. Figure 8(c) is when the angular velocity is maximum. The strong shear layer on the upper surface starts to separate from the trailing edge of the plate. Figure 8(d) shows the vortices when the plate near the cusp as labeled in the trajectory plot (Fig.7(b)). At this moment, a new generated clockwise LEV can be seen due to the rotation of the plate. In between the two vortices on the upper side of the plate, a high speed jet with low vorticity is formed, pointing to the location close to the one-quarter chord length. As shown in figure 8(e), merged with the shear layer on the upper surface, the generated clockwise LEV pushes the counterclock wise vortex upwards. The jet is now pointing to the mid-chord of the plate, and is separated by the upper shear layer. Figures 8(f)-8(h) finish the rest of cycle in which the plate flutters to the left.

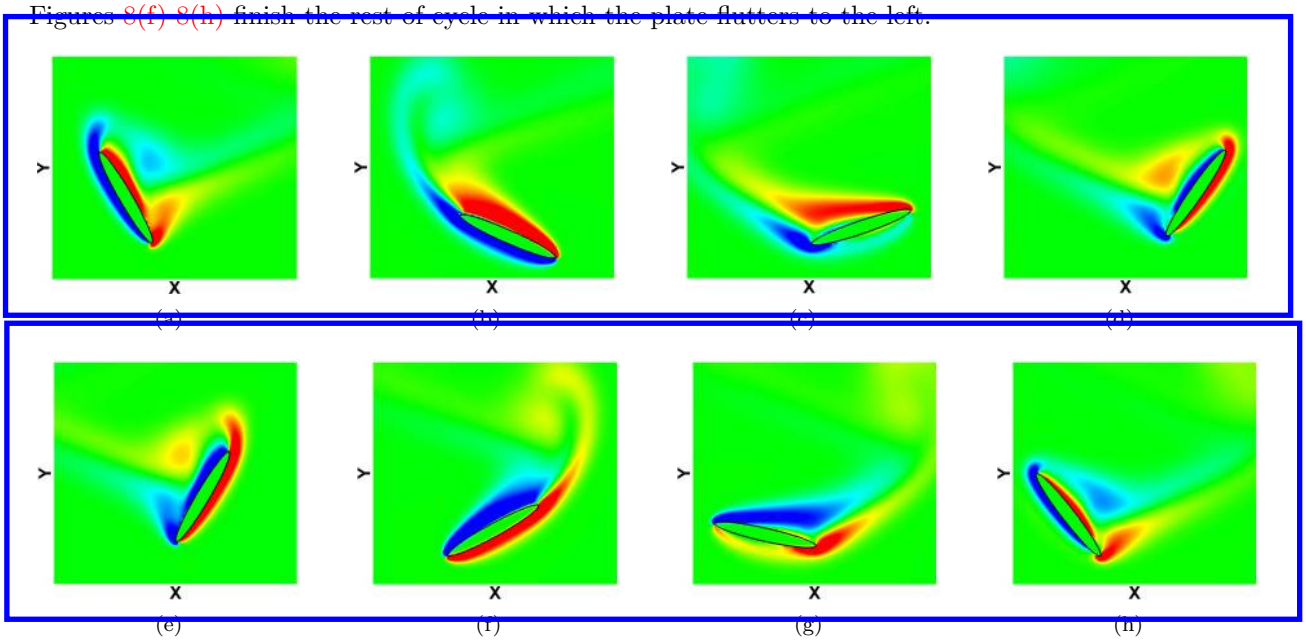

Figure 8. Vortex structure generated by a fluttering plate $F_r = 0.45$, $\theta_0 = 45^\circ$

The time course of aerodynamic force and the components are shown in figure 9 for plates in steady fluttering. The forces have been decomposed into the normal pressure (with subscript p) and viscous shear force (with subscript s). The horizontal force is plotted with the vertical speed V to emphasize the correlation between them. Similarly, the vertical force is plotted with the horizontal speed U. As shown in figure 9(a), during most of the time, the horizontal force coefficient C_X is dominated by its normal pressure component

C_{Xp}, which has two peaks during each half cycle of fluttering. One peak of C_{Xp} is correlated to the minimum |V|, where the plate stalls right before it reaches the cusp in the flutter trajectory. C_{Xp} brakes the horizontal motion of the plate since it is in the opposite direction to U. The second peak in C_{Xp} and C_X is generated when |V| reaches maximum, before which the plate has been accelerated after it passed the cusp. Note that C_{Xp} and U are in the same direction after the plate passing the cusp. The viscous shear force C_{Xs} gets its maximum in magnitude and dominates in C_X when the plate passes through the lateral symmetric line of fluttering trajectory, at which C_{Xp} is close to zero in magnitude and experiences changing in direction. |U| is at its highest value when the plate passes through the lateral symmetric line. After which, the magnitude of stress C_{Xs} reduces because the speed |U| starts to decrease. The force in vertical direction is strongly correlated with the horizontal speed of the plate (figure 9(b)). Contributed mainly by C_{Yp}, the highest C_Y is obtained when U is the maximum. On the other hand, when U is around 0 (the plate is near the cusp), C_Y reaches the minimum. The force component C_{Yp} is comparable to C_{Ys} when the plate is near the cusp. The aerodynamic moment and its components are presented in figure 9. The pressure component C_{Mp} leads Ω by a certain phase, indicating that the plate rotation is driven by C_{Mp}. It should be noted that the magnitude of shear stress induced moment is about 1/3 of that of pressure induced moment. Thus, the moment generated from shear stress is not negligible.

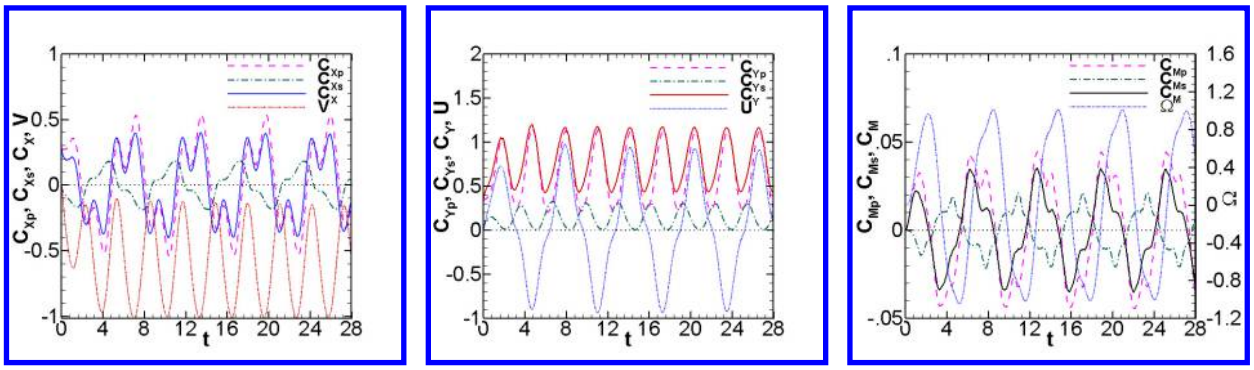

(a) Horizontal force and its components (b) Vertical force and its components (c) Moment and its components

Figure 9. Force history of a fluttering plate, $F_r = 0.45$, $\theta_0 = 45^\circ$

III.D. Transient process prior to tumbling

The transient process of a heavy plate prior to tumbling can be more complex than the transient process before fluttering of a light plate. Depending on the initial inclination angle θ_0, the plate may tumble to either the left or right side. As shown in figure 10, a plate with initial angle 45° makes flutter first before eventually tumbles. Figure 10(a) shows the velocity variation, and figure 10(b) shows the corresponding locations of the plate. Recalled that the forces F_X and F_Y are inversely proportional to the Froude number right after the plate is released, the F_X for a heavy plate is smaller than that of a light plate, and F_Y for a heavy plate is greater compared to that of a light plate. This explains why the heavy plate drops faster than the light plate after release.

The vorticity development of a plate in transient descent prior to tumbling is shown in figure 11. Figure 11(a) is taken when the vertical speed gets the maximum value after release. Figure 11(b) shows the vortices when the angular velocity of the plate obtains the maximum. In contrast to figure 6(e), the leading edge vortex of the heavy plate is much weaker. Figure 11(c) is taken when the angular velocity of the plate is instantaneously zero. The horizontal velocity U is locally maximum to the right at this moment, after which the horizontal speed decreases. Figure 11(d) is when the angular velocity of the plate reaches the maximum (in magnitude), at which the vortex separation can be seen on the upper side of the plate.

III.E. Steady tumbling

Figure 12(a) shows the time history of the velocity components in steady tumbling. It can be seen that the angular velocity Ω is inversely correlated with the vertical velocity component V. As the plate drops at a high magnitude of V, the angular velocity Ω is small, i.e., the plate is dominated by gliding motion. As the vertical speed of the plate is small (close to zero in this case), the plate rotates fast at the cusp where

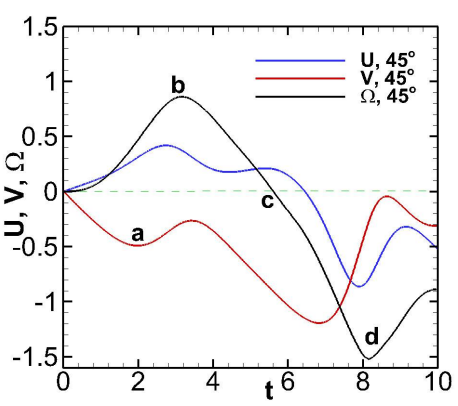

(a) Time history of velocity components

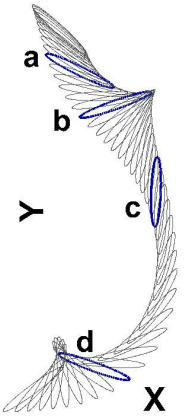

(b) Plate trajectory

Figure 10. A plate in transient process prior to tumbling, $F_r = 0.89$, $\theta_0 = 45°$.

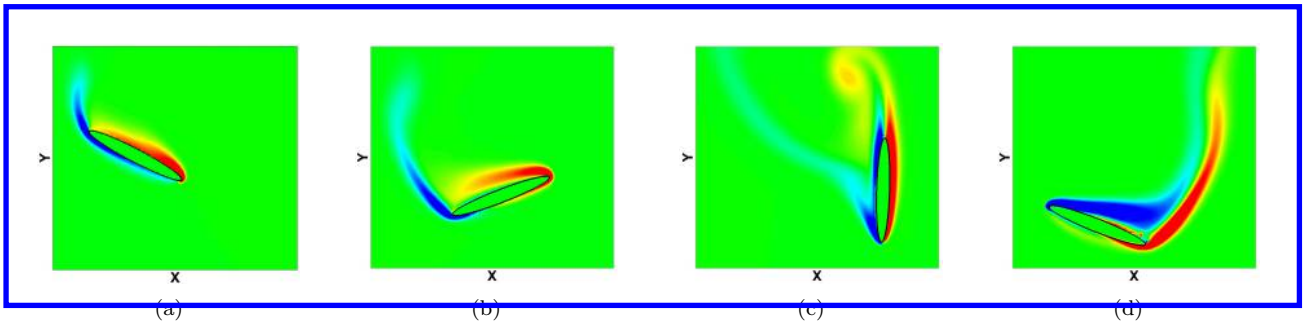

Figure 11. Vortices structure generated in transient process prior to tumbling, $F_r = 0.89$, $\theta_0 = 45°$.

the tumbling occurs. The vorticity snapshots of steady tumbling process are shown in figure 13, in which the corresponding position of the plate is labeled in figure 12(b). At position a, the plate is taking a high translational speed gliding. The jet induced by the leading and trailing edge vortices is located near the mid-chord of the plate, thus the angular velocity of the plate is minimum in magnitude. At position b, the motion of the plate is near the end of the gliding and the rotating process begins to dominate. The jet induced by the vortices from upper and lower surfaces is formed above the trailing edge. The plate rotates fast until it reaches position c, at which the angular velocity of the plate obtain its maximum value. The vortex layer on the upper surface now separates and a vortex is becoming formed at the advancing (trailing) edge. The position d corresponds to a position where the vertical speed is minimum, after which the plate starts to drop downwards with a certain acceleration.

The aerodynamic force history of the tumbling plate is presented in figure 14, with the subscripts p and s denoting the pressure and viscous force as in the fluttering case. It can be seen that the pressure component peak is one order of magnitude higher than the viscous component peak, in both X and Y directions. Although not exactly aligned up, C_{Xp} is correlated with V. The region near minimum |V| marks the fast revolving (tumbling) of the plate, in which high C_{Xp} is caused by the plate stall. From figure 14(a), during the periodic tumble, the viscous component C_{Xs} is always in the opposite direction of the plate drift direction (negative X). The positive C_{Xp} retards the horizontal drift of the plate, while the negative C_{Xp} accelerates the plate drifting. The correlation between C_{Yp} and U can be seen in figure 14(b), in which the maximum C_{Yp} is obtained when the horizontal speed U is high, and the minimum C_{Yp} is at where U is low. C_{Ys} is positive Y during the whole tumbling process, thus it provides part of the lift. At small U, C_{Ys} is in the same order of C_{Yp}. The moment component from surface pressure changes sign during the tumbling, thus it assists the rotation in certain portion of the cycle and prevents the rotation during the remainder. On the contrary, the moment generated by the shear force is generally in the opposite direction of rotation, and therefore prevents the rotation all the time.

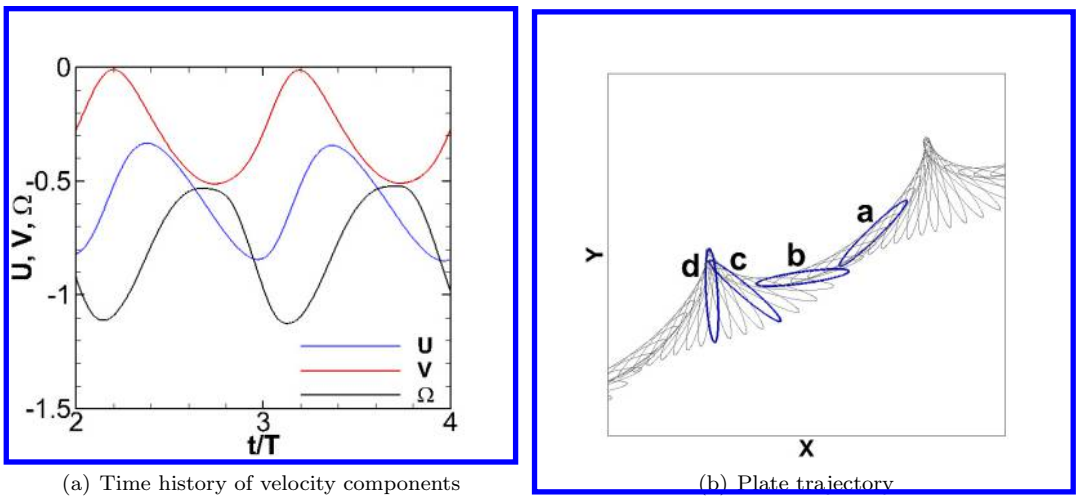

(a) Time history of velocity components (b) Plate trajectory

Figure 12. A plate in steady tumbling, $F_r = 0.89$, $\theta_0 = 45°$.

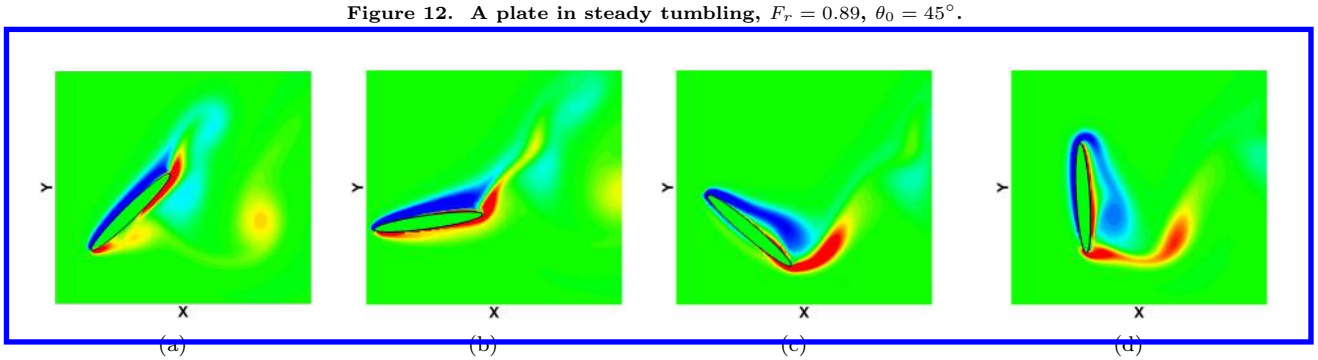

(a) (b) (c) (d)

Figure 13. Vorticity in steady tumbling, $F_r = 0.89$, $\theta_0 = 45°$

IV. Conclusion

Direct numerical simulation is carried out to study the transient process and periodic motion of fluttering and tumbling plates. During the transient process, instantaneous velocity of the plate can be either smaller or greater than terminal velocity (balanced by the buoyancy-modified gravity and aerodynamic force), depending on the initial inclination angle of the plate before release. At small inclination angles, the velocity (and acceleration) of the plate increases gradually, since the gravity must overcome high value of added mass induced by the acceleration of surrounding fluid. At high initial inclination angles, the added mass is small; the velocity of the plate can shoot up quickly and be greater than the terminal velocity of the plate. The high velocity will then be damped out by aerodynamic forces to obtain periodic fluttering or tumbling eventually. Meanwhile, the velocity and aerodynamic force components are cross-correlated during free flight, i.e., the high vertical force is coupled with the fast horizontal speed, and the high value of horizontal force is correlated with the fast speed in vertical direction. The aerodynamic moment generated by viscous force plays different roles in fluttering and tumbling. It can either assist or prevent the plate rotation in various stages of the fluttering. However, it can only prevent the plate rotation during tumbling.

Acknowledgments

This work is supported by AFOSR FA9550-11-1-0058 monitored by Dr. Douglas Smith and 2011 AFRL/RB summer faculty program monitored by Dr. Philip Beran at AFRL/RBSD.

References

[1]Maxwell, J. C., "On a particular case of the decent of a heavy body in a resisting medium," *Camb. Dublin Math. J.*, Vol. 9, 1853, pp. 145–148.

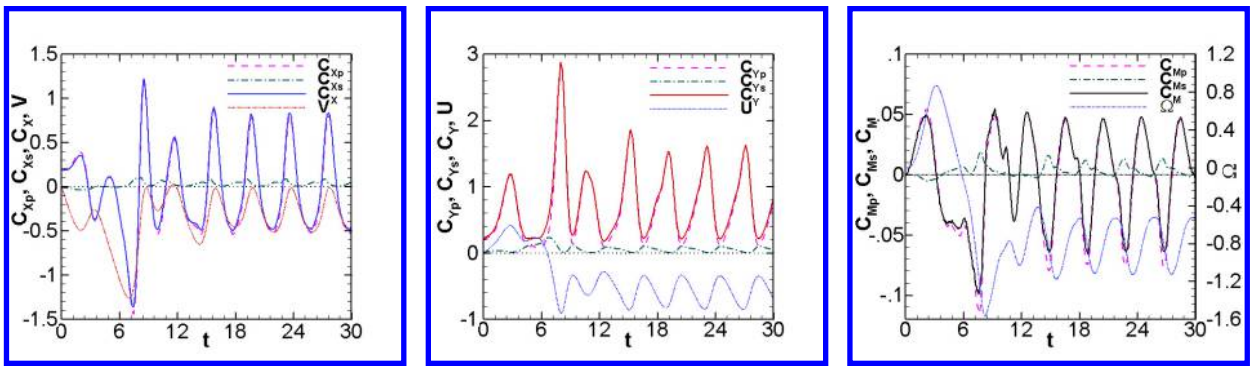

(a) Horizontal force and its components (b) Vertical force and its components (c) Moment and its components

Figure 14. Force history of a tumbling plate, $F_r = 0.89$, and $\theta_0 = 45°$.

[2]Willmarth, W. W., Hawk, N. E., and Harvey, R. L., "Steady and unsteady motions and wakes of freely falling disks," *Physics of Fluids*, Vol. 7, No. 2, 1964, pp. 197–208.

[3]Aref, H. and Jones, S. W., "Chaotic motion of a solid through ideal fluid," *Phys. Fluids A*, Vol. 5, No. 12, 1993, pp. 3026–3028.

[4]Field, S. B., Klaus, M., Moore, M. G., and Nori, F., "Chaotic dynamics of falling disks," *Nature*, Vol. 388, 1997, pp. 252–254.

[5]Belmonte, A., Elsenberg, H., and Moses, E., "From Flutter to Tumble: Inertial Drag and Froude Similarity in Falling Paper," *Physical Review Letters*, Vol. 81, No. 2, 1998, pp. 345–348.

[6]Andersen, A., Pesavento, U., and Wang, Z. J., "Unsteady aerodynamics of fluttering and tumbling plates," *J. Fluid Mech.*, Vol. 541, 2005, pp. 65–90.

[7]Andersen, A., Pesavento, U., and Wang, Z. J., "Analysis of transitions between fluttering, tumbling and steady descent of falling cards," *J. Fluid Mech.*, Vol. 541, 2005, pp. 91–104.

[8]Mittal, R., Seshadri, V., and Udaykumar, H., "Flutter, Tumble and Vortex Induced Autorotation," *Theoret. Comput. Fluid Dynamics*, Vol. 17, No. 3, 2004, pp. 165–170.

[9]Bonisch, S. and Heuveline, V., "On the numerical simulation of the unsteady free fall of a solid in a fluid: I. The Newtonian case," *Computers and Fluids*, Vol. 36, 2007, pp. 1434–1445.

[10]Jin, C. and Xu, K., "Numerical Study of the Unsteady Aerodynamics of Freely Falling Plates," *Commun. Comput. Phys.*, Vol. 3, No. 4, 2008, pp. 834–851.

[11]Jones, M. A. and Shelley, M. J., "Falling cards," *J. Fluid Mech.*, Vol. 540, 2005, pp. 393–425.

[12]Dong, H., Mittal, R., and Najjar, F. M., "Wake topology and hydrodynamic performance of low-aspect-ratio flapping foils," *J. Fluid Mech.*, Vol. 566, 2006, pp. 309–343.

[13]Mittal, R., Dong, H., , Bozkurttas, M., Najjar, F. M., Vargas, A., and von Loebbecke, A., "A versatile sharp interface immersed boundary method for incompressible flows with complex boundaries," *J. Computational Physics*, Vol. 227, 2008, pp. 4825–4852.